2001 IEEE Intelligent Transportation Systems Conference Proceedings - Oakland (CA), USA - August 25-29, 2001

DGPS/INS Integrated Positioning for Control of Automated Vehicle

Keith A. Redmill Takeshi Kitajima Ümit Özgüner

Department of Electrical Engineering
The Ohio State University
{redmill,umit}@ee.eng.ohio-state.edu

Abstract

In recent years, the Global Positioning System (GPS) has solidified its presence as a dependable means of navigation by providing absolute positioning in various applications. While GPS alone can provide position information, it has several weaknesses, such as low data output rate and vulnerability to external disturbances. We explore the feasibility of an integrated positioning system using a Differential GPS (DGPS) and an Inertial Navigation System (INS) for the control of an automated vehicle. An extended Kalman filter which combines the measurements from the DGPS, INS, and vehicle sensors to produce estimates of various vehicle states is derived. A methodology which, using map data, converts position measurements to vehicle lateral offset and desired speed, as applicable for the control of an automated vehicle, is presented. An analysis of the overall closed-loop vehicle control system is discussed. Finally, the performance of the proposed control scheme is examined through field tests conducted on two different vehicle platforms, an automated golfcart and a drive-by-wire Honda Accord sedan.

1 Introduction

Vehicle position sensors play a vital role in the success of automated vehicle control system operation, for the accuracy of the vehicle position measurement directly determines the reliability of the system under automated operation. Various classes of sensors are available to provide vehicle position information. Each class operates using different principles, and thus each has its own strengths and weaknesses. In selecting the position sensor or sensors for use in an automated vehicle, one must take into account the various operational factors of the sensor such as accuracy, repeatability, reliability, size, dynamic range, sensitivity, process requirement, and cost, and choose the sensor that is most appropriate for the application under consideration. Here, the importance of sensor redundancy must be stressed, for sensor failure, be it mechanical, electrical, or due to an external disturbance, could lead to disastrous results if the failed sensor was the only sensor on-board. Also, there should be a significant benefit in combining information from multiple sensors since each class of sensors has its own optimal operating condition within which it may outperform other sensors.

We explore the feasibility of employing a DGPS/INS integrated positioning system for the control of an automated vehicle. Unlike the sensor configurations implemented in other automated vehicle research such as vision, radar, or magnet based systems, which provide *relative* vehicle position information with respect to the roadway, the positioning system proposed here provides the vehicle with *absolute* position information. Given this fundamental distinction, the primary objective is to examine the performance of a DGPS/INS integrated positioning system combined with a map database to determine whether this approach is a viable option for automated vehicle control.

With this objective in mind, an integrated positioning system employing an extended Kalman filter is first developed. Position estimates are integrated with map data to provide an offset error signal. This information is used for the control of the automated vehicle.

2 Global Positioning System

The Global Positioning System, or GPS, is a satellite-based radio-navigation system which provides continuous, accurate, three-dimensional position and velocity information to the users of GPS receivers worldwide in all weather conditions. The underlying principle of GPS is the triangulation of position. If the distances from a point to three other non-coplanar points of known coordinates are given, the coordinates of the point can uniquely be determined, since the given information will comprise three equations to be solved for three unknowns. To compensate for receiver clock error, GPS uses not three, but four satellite-to-receiver ranges and locations to solve for an additional unknown, the clock offset.

2.1 Error Sources

The accuracy of GPS position measurements depends on the quality of the pseudorange measurements and satellite ephemeris data. The major sources of GPS error are Selective Availability, an intentional degradation of civilian GPS performance, atmospheric errors, including variable propagation rates and refractions, multipath errors, and satellite clock and ephemeris data errors. The error budget for these sources is shown in Table 1[1].

Error Source	GPS	DGPS
Satellite Clock	1.5	0
Orbit Error	2.5	0
Ionosphere	5.0	0.4
Troposphere	0.5	0.2
Receiver Noise	0.3	0.3
Multipath	0.6	0.6
Selective Availability	30	0

Table 1: Typical Error Budget (meters)

2.2 Differential GPS

Many of the errors outlined in the previous section are common to all receivers in a local geographic area. The

concept of Differential GPS (DGPS) utilizes this characteristic and attempts to compensate by using a base station situated at a precisely surveyed location. This base station, like all other receivers, receives signals from the satellites and determines the range errors by differencing the calculated and the measured ranges. These errors are broadcast to other receivers in the area so that they can correct their range measurements and consequently obtain position estimates of higher accuracy.

3 Inertial Navigation System

3.1 INS Overview

Inertial navigation is a form of the oldest navigation methods known to man, dead reckoning, where positions are calculated based on the distance and the direction of travel from a certain initial point. The *inertial measurement unit*, or IMU, which is composed of accelerometers and gyroscopes, is often used to obtain displacement and orientation measurements. In order to obtain navigational information in three-dimensional space, three accelerometers and three gyroscopes are required to account for the six spatial degrees of freedom.

3.1.1 Accelerometer

Accelerometers can be classified as either mechanical or semiconductor. A standard mechanical accelerometer consists of a proof mass balanced at an equillibrium position by the tension of a spring. When the case of the sensor is subjected to an acceleration along its sensitive axis, the proof mass is displaced with respect to its steady state position. The extension of the spring is related to the applied force, which is proportional to the acceleration.

The solid-state accelerometers used in this research employ a Wheatstone Bridge consisting of semiconductor strain gauges. The gauges are bonded to a cantilever beam which has a seismic mass attached at its end. When subjected to acceleration, the mass creates force which generates a bending moment in the beam, and this moment creates a strain which results in a bridge imbalance. This produces an output voltage proportional to the acceleration.

3.1.2 Gyroscope

Gyroscopes measure rotational rates around a sensitive axis. As with accelerometers, gyroscopes can be based on either mechanical or semiconductor technologies. Advances in semiconductor technology have led to the development of solid state devices such as magneto-hydrodynamic, electrostatic, vibratory, and optical rate sensors[2].

The gyroscopes used in this research are of the vibratory type, whose principle of operation is based on the Coriolis acceleration generated when a object undergoing vibratory motion is subjected to a rotational motion about an axis orthogonal to the linear velocity created by the oscillation. It consists of a triangular prism, with a piezoelectric transducer mounted on each face. Exciting one of these transducers provides the vibratory motion which is sensed by the other two transducers. Rotation of the prism about its principal axis creates Coriolis acceleration which affects the magnitude of the vibrations sensed by the transducers. Internal signal analysis circuitry generates an output voltage proportional to the angular velocity of the device[3].

3.2 Sensor Errors

As with any sensor, accelerometers and gyroscopes are subject to errors which limit the accuracy of their measurements. The major sources of error common in both accelerometers and gyroscopes are

- **Bias,**
- **Scale factor error,**
- **Cross coupling error,**
- **Alignment error,**
- **Measurement noise.**

Many of these errors are temperature dependent.

4 DGPS/INS Integration for Navigation

4.1 Motivation for Integration

As may be inferred from the descriptions of the previous sections, GPS and INS sensors have complementary characteristics. The characteristics which motivate the integration of these two sensors into a navigation system can be summarized as:

- **Accuracy** : Due to the integration process involved when providing a position estimate, an INS system can experience an unbounded growth of its error over time, even with high accuracy sensors. This gives rise to the need for an augmentation of the measurements by an external source which can periodically correct the errors. GPS, with its bounded measurement error, can be used to accomplish this.
- **Data Output Rate** : The data output rate of a GPS is generally 1 Hz, and at most 10 Hz, as in the DGPS receiver used in this research. This is insufficient for the control of a vehicle under autonomous control. The output rate of an INS can be much higher, the only limit being the computational capability of the data processing computer. The integration of GPS and INS measurements can therefore satisfy the data output rate requirement.
- **Data Availability** : GPS is a line-of-sight, radio-navigation system, and therefore GPS measurements are subject to signal outages, interference, and jamming, whereas INS is a self-contained that is (relatively) independent of the surrounding environment, and hence much more immune to external disturbances. Therefore, INS can continually provide navigation information when GPS experiences a short-term loss of signal.

It should now be clear, by examining the strengths and weaknesses of both systems, that integration of GPS and INS will lead to a more efficient, robust, and accurate position estimate.

4.2 Filter Configuration

Since the 1960's, the majority of researchers relied on Kalman filtering to obtain navigation solution from inertial measurements. Originally reported by R.E. Kalman in 1960, the Kalman filter is a method of obtaining optimal state estimates of a dynamical system in the presence of random processes. The Kalman filter is well known for

its superior performance in yielding the best estimates by blending redundant information from multiple sources[4].

The total state, or direct integration, concept followed in this research will now be stated. First, the main source of navigation will be measurements from the DGPS. This is a logical choice since the DGPS measurement that is available from the receiver used in this research has an accuracy of approximately ±1 meter. In contrast to the concept often used in DGPS/INS integration schemes, the *INS* measurements will be used to supplement the DGPS, or provide navigation solution between DGPS samples. However, this does not imply that the DGPS measurements will be considered perfect; enough autonomy will be preserved (through the tuning of the process noise variance parameters) so that INS measurements will influence the position estimates through the Kalman filter. This concept also provides smooth transitions from one DGPS sample to another, eliminating any discontinuities in position estimates.

4.3 Hardware Description

The INS employed in this research is comprised of two accelerometers and one gyroscope, allowing the estimation of position in two dimensional space. Of the three rotational motions the vehicle experiences (yaw, pitch, and roll), only yaw is considered since this is the only information necessary to resolve navigation information in two dimensions. Below are brief descriptions of the instruments used for the experiments on the golfcart and the automobile platforms.

4.3.1 DGPS Receiver

The DGPS receiver used for this research is the AgGPS-132 manufactured by Trimble Navigation Ltd. It features a combined GPS/DGPS antenna with 12 GPS tracking channels, and is capable of receiving both radiobeacon and satellite differential corrections to achieve submeter accuracy. The satellite corrections will be provided by the OmniSTAR wide-area differential GPS service. It will be interfaced to a computer through an RS-232 serial link and will output position data at the rate of either 1, 5, or 10 Hz.

4.3.2 Accelerometer

The accelerometers used in the x and y direction are the EGCS-A2-2 accelerometer manufactured by ENTRAN Devices Ltd. The maximum range is ±2 g (19.6 m/s^2).

4.3.3 Gyroscope

The Gyrostar ENV-05D-52 piezoelectric gyroscope manufactured by Murata will be used to measure the yaw rate of the vehicle. The maximum range is ± 80 deg/sec.

4.4 INS Error Modelling

The greatest challenge in implementing an inertial navigation system is the development of the error dynamics models. To develop error models for both the accelerometers and the gyroscope, their outputs were recorded over a period of 30 minutes while stationary on the laboratory bench. The sensors exhibit measurement noise as well as a large, slowly time-varying bias which is attributed to the thermal effects of the internal circuitry of the device. For the inertial sensors, the associated error will be represented as

$$\epsilon = \epsilon_b + \nu \tag{1}$$

where ϵ_b is the random bias and ν is the measurement noise. The equation describing the dynamics of this error is simply

$$\dot{\epsilon}_b = 0 \tag{2}$$

The simplicity of the above error model is rewarded as computational efficiency and is justified by the fact that it will be incorporated in the Kalman filter in direct configuration.

4.5 Filter Design

The design of a Kalman filter involves the derivation of state equations incorporating the dynamics of the system whose states are to be estimated and the formulation of the observation equations. An extended Kalman filter will be implemented.

4.5.1 Observation Equations

The sources of position information in this research are the DGPS and the INS. The measurements available from the DGPS are latitude, longitude, velocity, and absolute heading angle. After proper coordinate transformations, these can give the position and velocity along the eastern and northern axes of the tangent plane coordinate frame. The observation available from INS are the yaw rate and the acceleration in the two-dimensional vehicle frame. This will lead to the nonlinear discrete-time observation equations

$$z_e(k) = e(k) + \nu_e(k) \tag{3}$$
$$z_n(k) = n(k) + \nu_n(k) \tag{4}$$
$$z_{v_e}(k) = v_e(k) + \nu_{v_e}(k) \tag{5}$$
$$z_{v_n}(k) = v_n(k) + \nu_{v_n}(k) \tag{6}$$
$$z_\psi(k) = \psi(k) + \nu_\psi(k) \tag{7}$$
$$z_{\dot\psi}(k) = \dot\psi(k) + \epsilon_{\dot\psi}(k) + \nu_{\dot\psi(k)} \tag{8}$$
$$z_{a_x}(k) = \sin(\psi(k))a_e(k) - \cos(\psi(k))a_n(k) + \epsilon_{a_x}(k) + \nu_{a_x}(k) \tag{9}$$
$$z_{a_y}(k) = \cos(\psi(k))a_e(k) + \sin(\psi(k))a_n(k) + \epsilon_{a_y}(k) + \nu_{a_y}(k) \tag{10}$$

The first five equations are the observations from the DGPS and the last three are from the inertial sensors. In the above equations, $e(k)$, $n(k)$, $v_e(k)$, $v_n(k)$, $a_e(k)$, and $a_n(k)$ denote the position, velocity, and acceleration along the eastern and northern axes of the tangent plane coordinate frame, respectively, $\psi(k)$ is the heading angle with respect to true east, $\dot\psi$ is its derivative or the yaw rate, and ν_* denote the associated measurement noise. As can be observed from Equations (9) and (10), the accelerations in the tangent plane, namely $a_e(k)$ and $a_n(k)$, are related to the accelerations $z_{a_x}(k)$ and $z_{a_y}(k)$ measured in the vehicle frame by the tangent plane to vehicle frame transformation through the heading angle $\psi(k)$. Finally, $\epsilon_{\dot\psi}$, ϵ_{a_x} and ϵ_{a_y} are the random biases in the yaw rate, x acceleration, and y acceleration measurements defined in vehicle coordinates, which will be modelled as in Equation (2).

Quite naturally, the nonlinearity of the observation equations (9) and (10) implies the use of an extended Kalman filter whose observation equation is written in matrix form as

$$\mathbf{z}(k) = \mathbf{h}[\mathbf{x}(k)] + \boldsymbol{\nu}(k) \tag{11}$$

The states of the system will now be defined in a manner that will allow Equations (3) through (10) to be expressed in this form.

4.5.2 State Equations

The state equations will be derived in continuous-time and then discretized. For clarity, the dynamics of the gyroscope measurements will be considered first.

Incorporating the error model derived in Equation (2), the continuous-time model of the gyroscope can be represented in matrix notation as

$$\dot{\mathbf{x}}_\psi(\mathrm{t}) = \mathbf{A}_\psi(\mathrm{t})\mathbf{x}_\psi(\mathrm{t}) + \mathbf{w}_\psi(\mathrm{t}) \tag{12}$$

where

$$\mathbf{A}_\psi = \begin{bmatrix} 0 & 1 & 0 \\ 0 & 0 & 0 \\ 0 & 0 & 0 \end{bmatrix}, \quad \mathbf{x}_\psi(\mathrm{t}) = \begin{bmatrix} \psi(t) \\ \dot{\psi}(t) \\ \epsilon_{\dot{\psi}}(t) \end{bmatrix} \tag{13}$$

$$\mathbf{w}_\psi(\mathrm{t}) = \begin{bmatrix} 0 \\ w_{\dot{\psi}}(t) \\ w_{\epsilon_{\dot{\psi}}}(t) \end{bmatrix} \quad \boldsymbol{\Upsilon}_\psi(\mathrm{t}) = \begin{bmatrix} 0 & 0 & 0 \\ 0 & \sigma^2_{\dot{\psi}} & 0 \\ 0 & 0 & \sigma^2_{\epsilon_{\dot{\psi}}} \end{bmatrix} \tag{14}$$

The state vector for the gyroscope is composed of the orientation angle ψ, the yaw rate $\dot{\psi}$, and the random bias $\epsilon_{\dot{\psi}}$. Here, $\mathbf{w}_\psi(\mathrm{t})$ is assumed to be a white process noise vector that is taken to be the input which drives the yaw rate and the random bias, and $\boldsymbol{\Upsilon}_\psi(\mathrm{t})$ is its associated continuous-time process noise covariance matrix. The elements of $\boldsymbol{\Upsilon}_\psi(\mathrm{t})$, $\sigma^2_{\dot{\psi}}$, and $\sigma^2_{\epsilon_{\dot{\psi}}}$ denote the variance of the process noise associated with the yaw rate and the random bias, respectively.

Discretization in the standard manner leads to the discrete-time state equation

$$\mathbf{x}_\psi(\mathrm{k}+1) = \boldsymbol{\Phi}_\psi(\mathrm{k})\mathbf{x}_\psi(\mathrm{k}) + \mathbf{w}_\psi(\mathrm{k}) \tag{15}$$

where

$$\boldsymbol{\Phi}_\psi = \begin{bmatrix} 1 & T_s & 0 \\ 0 & 1 & 0 \\ 0 & 0 & 1 \end{bmatrix} \quad \mathbf{x}_\psi(\mathrm{k}) = \begin{bmatrix} \psi(k) \\ \dot{\psi}(k) \\ \epsilon_{\dot{\psi}}(k) \end{bmatrix}. \tag{16}$$

In Equation (16), T_s is the sampling interval. The discrete-time process noise covariance matrix $\mathbf{Q}_\psi(\mathrm{k})$ is derived from its continuous-time counterpart $\boldsymbol{\Upsilon}_\psi(\mathrm{t})$ as [5]

$$\mathbf{Q}_\psi(\mathrm{k}) = \int_{t_k}^{t_{k+1}} e^{\mathbf{A}_\psi(\mathrm{t_{k+1}}-\tau)} \boldsymbol{\Upsilon}_\psi(\tau) \mathrm{e}^{\mathbf{A}^{\mathrm{T}}_\psi(\mathrm{t_{k+1}}-\tau)} \mathrm{d}\tau \tag{17}$$

$$= \int_{t_k}^{t_{k+1}} \begin{bmatrix} 1 & t_k-\tau & 0 \\ 0 & 1 & 0 \\ 0 & 0 & 1 \end{bmatrix} \begin{bmatrix} 0 & 0 & 0 \\ 0 & \sigma^2_{\dot{\psi}} & 0 \\ 0 & 0 & \sigma^2_{\epsilon_{\dot{\psi}}} \end{bmatrix} \begin{bmatrix} 1 & 0 & 0 \\ t_k-\tau & 1 & 0 \\ 0 & 0 & 1 \end{bmatrix} d\tau \tag{18}$$

$$= \begin{bmatrix} \frac{1}{3}T_s^3\sigma^2_{\dot{\psi}} & \frac{1}{2}T_s^2\sigma^2_{\dot{\psi}} & 0 \\ \frac{1}{2}T_s^2\sigma^2_{\dot{\psi}} & T_s\sigma^2_{\dot{\psi}} & 0 \\ 0 & 0 & T_s\sigma^2_{\epsilon_{\dot{\psi}}} \end{bmatrix} \tag{19}$$

Defining the remaining states as

$$\mathbf{x}_{\mathrm{e,x}}(\mathrm{k}) = \begin{bmatrix} e(k) \\ v_e(k) \\ a_e(k) \\ \epsilon_{a_x}(k) \end{bmatrix} \qquad \mathbf{x}_{\mathrm{n,y}}(\mathrm{k}) = \begin{bmatrix} n(k) \\ v_n(k) \\ a_n(k) \\ \epsilon_{a_y}(k) \end{bmatrix} \tag{20}$$

discrete-time state equations similar to that of the gyroscope measurements can be derived. The states in Equation (20) are as defined in the subsection on observation equations. The subscripts in the above state vectors indicate that the first three states, the position, velocity, and acceleration, are all defined in the tangent plane coordinate frame whereas the last state, the accelerometer error, is defined in the vehicle coordinate frame.

The state equation combining all of the states can now be presented in block matrix form.

$$\begin{bmatrix} \mathbf{x}_\psi(\mathrm{k}+1) \\ \mathbf{x}_{\mathrm{e,x}}(\mathrm{k}+1) \\ \mathbf{x}_{\mathrm{n,y}}(\mathrm{k}+1) \end{bmatrix} = \begin{bmatrix} \boldsymbol{\Phi}_\psi & \mathbf{0} & \mathbf{0} \\ \mathbf{0} & \boldsymbol{\Phi}_{\mathrm{e,x}} & \mathbf{0} \\ \mathbf{0} & \mathbf{0} & \boldsymbol{\Phi}_{\mathrm{n,y}} \end{bmatrix} \begin{bmatrix} \mathbf{x}_\psi(\mathrm{k}) \\ \mathbf{x}_{\mathrm{e,x}}(\mathrm{k}) \\ \mathbf{x}_{\mathrm{n,y}}(\mathrm{k}) \end{bmatrix} + \mathbf{w}(\mathrm{k}) \tag{21}$$

where

$$\boldsymbol{\Phi}_{\mathrm{e,x}} = \boldsymbol{\Phi}_{\mathrm{n,y}} = \begin{bmatrix} 1 & T_s & \frac{1}{2}T_s^2 & 0 \\ 0 & 1 & T_s & 0 \\ 0 & 0 & 1 & 0 \\ 0 & 0 & 0 & 1 \end{bmatrix}, \tag{22}$$

Φ_ψ is as defined in Equation (16), and $\mathbf{w}(\mathrm{k})$ is the process noise vector. From Equation (17), the process covariance matrix can be expressed as

$$\mathbf{Q}(\mathrm{k}) = \begin{bmatrix} \mathbf{Q}_\psi & \mathbf{0} & \mathbf{0} \\ \mathbf{0} & \mathbf{Q}_{\mathrm{e,x}} & \mathbf{0} \\ \mathbf{0} & \mathbf{0} & \mathbf{Q}_{\mathrm{n,y}} \end{bmatrix} \tag{23}$$

where

$$\mathbf{Q}_{\mathrm{e,x}} = \begin{bmatrix} \frac{1}{20}T_s^5\sigma^2_{a_x} & \frac{1}{8}T_s^4\sigma^2_{a_x} & \frac{1}{6}T_s^3\sigma^2_{a_x} & 0 \\ \frac{1}{8}T_s^4\sigma^2_{a_x} & \frac{1}{3}T_s^3\sigma^2_{a_x} & \frac{1}{2}T_s^2\sigma^2_{a_x} & 0 \\ \frac{1}{6}T_s^3\sigma^2_{a_x} & \frac{1}{2}T_s^2\sigma^2_{a_x} & T_s\sigma^2_{a_x} & 0 \\ 0 & 0 & 0 & T_s\sigma^2_{\epsilon_{a_x}} \end{bmatrix} \tag{24}$$

$$\mathbf{Q}_{\mathrm{n,y}} = \begin{bmatrix} \frac{1}{20}T_s^5\sigma^2_{a_n} & \frac{1}{8}T_s^4\sigma^2_{a_n} & \frac{1}{6}T_s^3\sigma^2_{a_n} & 0 \\ \frac{1}{8}T_s^4\sigma^2_{a_n} & \frac{1}{3}T_s^3\sigma^2_{a_n} & \frac{1}{2}T_s^2\sigma^2_{a_n} & 0 \\ \frac{1}{6}T_s^3\sigma^2_{a_n} & \frac{1}{2}T_s^2\sigma^2_{a_n} & T_s\sigma^2_{a_n} & 0 \\ 0 & 0 & 0 & T_s\sigma^2_{\epsilon_{a_y}} \end{bmatrix} \tag{25}$$

and $\mathbf{Q}_\psi$ is as defined in Equation (19). In the above matrices, $\sigma^2_{a_e}$, $\sigma^2_{a_n}$, $\sigma^2_{\epsilon_{a_x}}$ and $\sigma^2_{\epsilon_{a_y}}$ represent the variance of the process noise associated with the eastern and northern acceleration and the random bias of x and y accelerometers, respectively.

4.6 Filter Analysis

Now that the state equations are defined and the algorithm of the extended Kalman filter outlined, some analysis of the filter can be made by examining the observation equations. As mentioned in Section 4.5.1, the accelerometer measurements are related to the acceleration in the tangent plane coordinate frame by coordinate transformation (i.e. Equations (9) and (10)), and the acceleration in the tangent plane coordinate frame are related to the eastern and northern position via the state equation, which in turn, are related to the DGPS measurements through the observation equations, thereby building a link between DGPS and INS measurements. This is how the blending of the measurements is carried out in the Kalman filter. The extent of this blending is determined by the Kalman gain $\mathbf{K}$ which is dependent on the error covariance matrix $\mathbf{P}$ and the measurement error covariance matrix $\mathbf{R}$.

Therefore, although the elements of **P** and **R** will be determined experimentally, the blending factor can be changed by varying the elements of these matrices.

The integrated DGPS/INS estimates were tuned by changing the DGPS measurement noise variance so that the estimates provide smooth interpolation between points within the predetermined DGPS measurement error bound. The same method of tuning can be carried out by varying the process noise variance, but variance estimates available from the stationary test data were used in this implementation.

5 Reference Path Tracking Control

For an automated vehicle to follow a prescribed path, information regarding the position of the vehicle with respect to the reference path is necessary. The information commonly used in the lateral control of a vehicle is the offset from the center of the road of a point along the longitudinal axis of the vehicle at some look-ahead distance. Vision, radar, magnetic marker, and magnetic tape sensor systems have been proposed. Similar to the approach taken for vision and radar based systems, the lateral vehicle controller considered here will use the offset measurement from the reference path at certain look-ahead distance along the longitudinal axis of the vehicle as its input. This section will discuss issues related to obtaining this error signal and the closed-loop control system.

5.1 Map Database Structure

In order to obtain the offset of the look-ahead point with respect to the reference path, a map database which contains information regarding the reference path must first be established. The database is comprised of line segments specified as set of points which define the reference path along with an associated desired speed.

5.2 Offset Calculation

The equation of a road segment will be represented as

$$ae + bn + c = 0 \tag{26}$$

where e and n denote the east and north coordinates in the tangent plane, and a, b, and c are parameters to be derived from the map data. They are given as

$$a = n_s - n_e \tag{27}$$
$$b = e_e - e_s \tag{28}$$
$$c = (n_e - n_s)e_s - (e_e - e_s)n_s \tag{29}$$

where e_s, n_s, e_e, and n_e denote the east and north coordinates of the start and end points of the segment, respectively. If the ID of the segment closest to the look-ahead point is known, the parameters of the equation for the corresponding segment can be used to calculate the offset $o(t)$, which is defined to be the shortest distance from the look-ahead point to the segment, using

$$o(t) = -sgn(s(t))\frac{|s(t)|}{\sqrt{a^2 + b^2}} \tag{30}$$

where

$$s(t) = ae_p(t) + bn_p(t) + c \tag{31}$$

and $e_p(t)$ and $n_p(t)$ denote the east and north position of the look-ahead point. These will be obtained from the vehicle position $(e(t), n(t))$ and orientation $\psi(t)$ using

$$e_p(t) = e(t) + d\cos(\psi(t)) \tag{32}$$
$$n_p(t) = n(t) + d\sin(\psi(t)) \tag{33}$$

where d is the look-ahead distance. The sign term in the offset will be employed to determine on which side of the reference path the look-ahead point lies, positive if on the right, and negative if on the left side. The definition of look-ahead offset is depicted in Figure 2.

5.3 Map Matching

In the previous subsection, the calculation of the offset assumed that the ID of the segment closest to the look-ahead point was known. The process of determining the segment on which the look-ahead point lies is called *map matching*, and is also employed in car navigation systems to reconcile the vehicle location with available map data.

5.4 Closed-Loop System

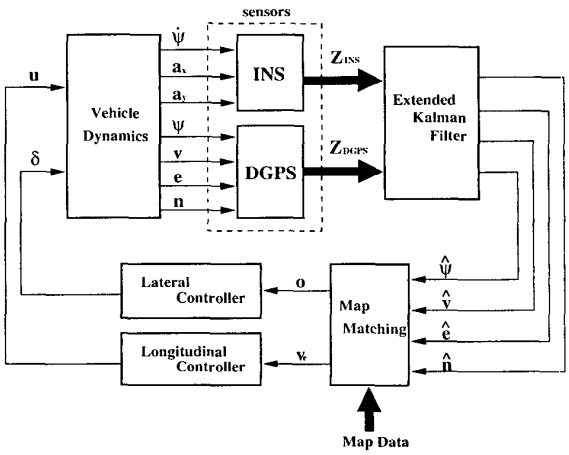

Figure 1: System Block Diagram

The closed-loop system based on the preceding discussions can be illustrated in the block diagram representation shown in Figure 1. The various states of the vehicle are measured by the sensors (i.e. INS and DGPS) and the measurements are fed into the extended Kalman filter where the optimal estimates of the vehicle states are computed. The estimates are then passed through the map matching function to obtain look-ahead offset and velocity error estimates which are the input to the lateral and longitudinal controllers. The resulting lateral and longitudinal commands are fed back into the vehicle to close the loop.

5.5 Control Algorithm

The algorithms presented in this work will be tested on two different vehicle platforms: a golfcart and an automobile. Due to the considerable differences in the vehicle dynamics of these platforms, different controllers were designed for each implementation. Details of the golfcart control are omitted from this document. The lateral and longitudinal controllers for the automobile are described in [6].

5.6 Analysis of Vehicle Stability

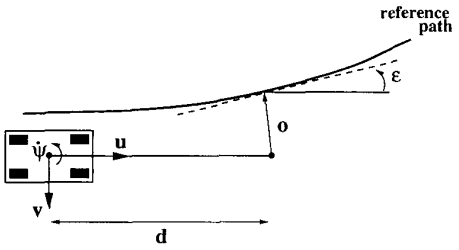

Figure 2: Look-ahead Offset Dynamics

The stability of the vehicle under automated path following control can be analyzed in the following manner[7]. As illustrated in Figure 2, the dynamics of the look-ahead offset can be written as

$$\dot{o}(t) = v(t) - \dot{\psi}(t)d + u\epsilon(t) \quad (34)$$

$$\dot{\epsilon}(t) = -\dot{\psi}(t) + uK \quad (35)$$

where o is the offset, d is the look-ahead distance, ϵ is the angle between the vehicle orientation and the road tangent at the look-ahead distance, and K is the road curvature which enters the system as a disturbance. Combining this system with a bicycle model (not described here) yields the system

$$\begin{bmatrix} \dot{v} \\ \ddot{\psi} \\ \dot{o} \\ \dot{\epsilon} \end{bmatrix} = \begin{bmatrix} -\frac{k_f+k_r}{mu} & u + \frac{ak_f - bk_r}{mu} & 0 & 0 \\ \frac{ak_f - bk_r}{I_z u} & -\frac{a^2k_f + b^2k_r}{I_z u} & 0 & 0 \\ 1 & -d & 0 & u \\ 0 & -1 & 0 & 0 \end{bmatrix} \begin{bmatrix} v \\ \dot{\psi} \\ o \\ \epsilon \end{bmatrix} + \begin{bmatrix} -\frac{k_f}{m} \\ \frac{ak_f}{I_z} \\ 0 \\ 0 \end{bmatrix} \delta + \begin{bmatrix} 0 \\ 0 \\ 0 \\ u \end{bmatrix} K$$

$$y = \begin{bmatrix} 0 & 0 & 1 & 0 \end{bmatrix} \begin{bmatrix} v \\ \dot{\psi} \\ o \\ \epsilon \end{bmatrix} \quad (36)$$

whose transfer function represents the relationship between the steering angle δ and the look-ahead offset o. Bode plots of the closed-loop system with the augmented vehicle model, lateral controller, and the steering actuator for various look-ahead distances are shown in Figure 3. Note that, for this analysis, parameters of the full-sized automobile are used and the controller is assumed to be a PID controller.

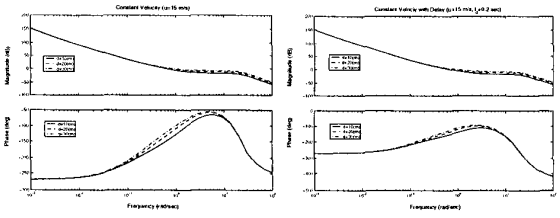

Figure 3: Bode Plots (left: constant velocity, right: constant velocity with delay)

At a constant longitudinal velocity of 15 m/sec, the left figure shows that increasing the look-ahead distance adds a substantial phase lead, making the closed-loop system more stable.

The right figure shows the Bode plot of the closed-loop system when a delay of 200 msec is taken into account. The GPS receiver used in this work is known to have approximately 100 msec of latency, and although the exact processing delay of the integrated position estimation system was not explicitly determined, this figure shows that phase lag introduced by delays can be compensated by increasing the look-ahead distance, thereby maintaining the stability of the closed-loop system.

6 Experimental Work

This section discusses the issues involved in the actual implementation of the navigation and control methods described in the previous sections. The details regarding the software are first treated, followed by the description of the hardware and the experimental results on both vehicle platforms.

6.1 Real-Time Software Implementation

For the automated vehicle control experiments conducted on the golfcart and the automobile, an Intel-based computer running the QNX real-time operating system was employed to perform all required data acquisition, vehicle state estimation, actuator control, and graphical user interface support tasks. A modular software architecture was utilized[6].

6.2 Automobile Hardware

The vehicle platform used was a 1996 Honda Accord LX sedan which was implemented as the Ohio State University Autonomous Vehicle for the NAHSC 1997 Technical Feasibility Demonstration held in San Diego, California. The specific details regarding the hardware on-board this vehicle can be found in [6].

6.3 Experimental Results

Automated control for the Honda Accord vehicle was tested at the Transportation Research Center in Marysville, Ohio on two different test courses. The first course was the Skid Pad, an approximately 1.2 mile stretch of multilane straight road, and the second course was the Widing Road Course, consisting of several curves of various curvature and straight subsections. The test on the Skid Pad challenged the automated control at highway speeds, whereas the test on the Winding Road Course allowed the examination of path tracking performance through a series of tight curves at high lateral accelerations and yaw rates.

The reference path tracking performance at highway speed was tested on the Skid Pad, with results such as those shown in Figure 4. The velocity profile plot reveals that the automated vehicle gradually accelerated from a stop to the top speed of 27 m/sec ($\approx$ 60 mph). The vehicle displayed satisfactory lane keeping ability, maintaining the tracking error to less than ± 0.5 meters after the start-up transients.

The results from an experiment conducted on the Winding Road Course are shown in Figures 5 and 6. For reference, in addition to the velocity profile and the tracking error, Figure 5 includes a plot of the road curvature. From the three plots it can be observed that the automated vehicle reached its top speed of 15 m/sec on the straight subsection and went through all of the curves at about

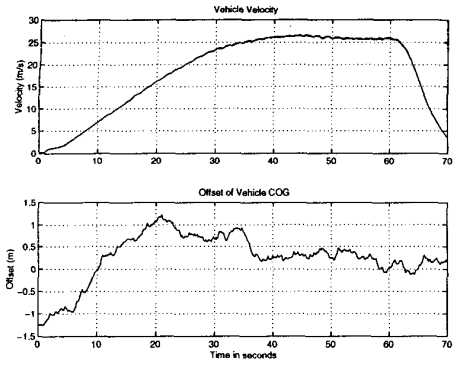

Figure 4: Skid Pad Experiment Results

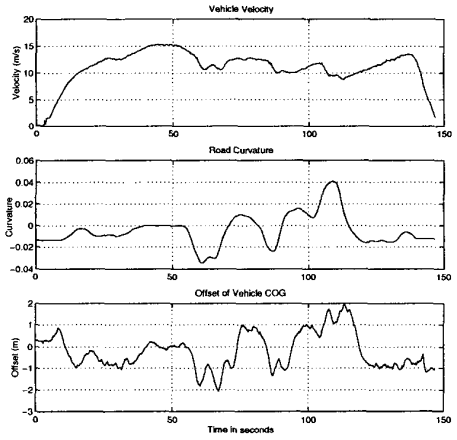

Figure 5: Winding Road Course Experiment Results

10 m/sec, during which the offset of the vehicle from the center of the lane was kept to within 2 meters.

It should be noted that in both tests, the ride was very smooth, free of jerky steering behavior. This is a design feature of the controller, and results in some decrease in absolute path tracking accuracy.

6.4 Conclusion on Tracking Performance

In conducting the field experiments on both vehicle platforms, it was seen that the tracking performance depended on parameter values, with the most critical parameter being the look-ahead distance. A poor choice of parameters could lead to persistent oscillations and even instability. In the experiments with a Honda Accord, a different set of controller gains and look-ahead distance were required for the two different test courses, implying the need for the lateral controller to take into consideration the vehicle velocity, the look-ahead distance, and the expected road curvature. Nevertheless, the field experiments verified that the DGPS/INS integrated positioning system and the control scheme proposed in this work is in fact feasible for implementation in the control of automated vehicles.

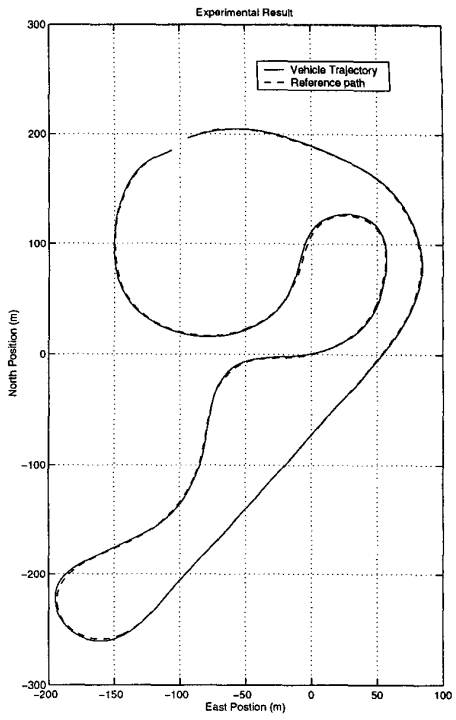

Figure 6: Winding Road Course Vehicle Trajectory

References

[1] Trimble Navigation Ltd., *How GPS Works: A Tutorial.* http://www.trimble.com/gps/.

[2] D. H. Titterton and J. L. Weston, *Strapdown Inertial Navigation Technology.* Stevenage, United Kingdom: Peter Peregrinus Ltd., 1997.

[3] B. Barshan and H. F. Durrant-Whyte, "Inertial navigation systems for mobile robots," *IEEE Transactions on Robotics and Automation*, vol. 11, pp. 328–342, June 1995.

[4] R. R. Brooks, *Multi-sensor fusion : fundamentals and applications with software.* Englewood Cliffs, NJ: Prentice-Hall Inc., 1998.

[5] C. A. Scott, *Improved Positioning of Motor Vehicles Through Secondary Information Sources.* PhD thesis, University of Technology, Sydney, 1996.

[6] K. A. Redmill, *Automated Vehicles: The Nature and Implementation of Autonomous Multi-Agent Systems.* PhD thesis, The Ohio State University, 1998.

[7] J. Kosecka, R. Blasi, and J. Malik, "A comparative study of vision-based lateral control strategies for autonomous highway driving," *The International Journal of Robotic Research*, vol. 18, pp. 442–453, May 1999.